Fast-Field Cycling Nuclear Magnetic Resonance relaxometer's magnet with optimized homogeneity and reduced volume

Extended abstract

Pedro Videira[1],
[1] *CeFEMA, Departamento de Física, Instituto Superior Técnico – IST, Universidade de Lisboa – UL, Avenida Rovisco Pais 1, 1049 Lisboa, Portugal*
(Dated: September 2017)

In this article a new Fast Field Cycling (FFC) Nuclear Magnetic Resonance (NMR) electromagnet with low power consumption (less than 200 W), high field homogeneity and reduced volume is projected and described. The electromagnet is made of iron, possessing a high permeability and allowing for good magnetic field homogeneity in the operating range of 0 to 0.33 T. Electromagnet's experimental results and simulation using COMSOL Multiphysics® evaluating the generated magnetic field, field homogeneity, heating effects and cooling requirements are presented. The required coupled systems such as the cooling, sample heating are assessed and projected.

I. INTRODUCTION

Nuclear magnetic resonance spectroscopy is a experimental technique that makes use of the magnetic properties of certain atomic nuclei in order to determine physical and chemical characteristics of atoms and/or molecules in which they are contained. It is a powerful and broad technique that has constantly evolved thanks to the use of new power semi-conductors, new materials and optimization techniques.

A FFC NMR spectrometer is basically constituted by an electromagnet and a power supply that is able to perform fast switching of the magnetic field between defined values. With the development of more powerful and reliable FFC spectrometers efforts have been devoted to decrease size and power requirements of the equipments while increasing its portability.

There are different FFC NMR equipments available usually with air-core and copper or aluminium solenoid coils designed to produce high homogeneity magnetic fields. A special requirement of FFC is fast switching of magnetic fields with reasonable supply voltages. This usually requires low self-inductance and low resistance leading to electromagnets supplied with high current. Such features require cooling systems capable of dissipating up to several kilowatts.

Temperature fluctuations of the system lead to changes in the magnets ohmic resistance affecting field values and switching times making FFC experiments very sensitive to the temperature stability of the electromagnets. In some cases the cooling system isn't capable of stabilizing the temperature in long periods of time introducing the necessity of cooling periods where the current is turned to zero or low values. This "off" periods represent a constrain in samples where the magnetic induced alignment is important aspect such as liquid crystals. This work arises in order to try to overcome the current restraints that characterize the state-of-the-art FFC spectrometers.

Whereas high resolution Nuclear magnetic resonance and Magnetic resonance imaging have become highly desired tools in the non-academic world Field Cycling relaxometry has not. Energy efficient, compact, cheap and portable equipments are not yet commercially available, while the existing ones do not possess all the desired qualities. A growing interest and new possible applications is observed for NMR motivating the research on developing new and more suitable equipments on what is believed to be, a superior technique. In this paper a low-power FFC NMR electromagnet is simulated using COMSOL Multiphysics®, projected and described as well as the sample heating and cooling systems. This is the smallest iron electromagnet built up-to-date by the group of Complex Fluids NMR and surfaces.

II. THEORETICAL BACKGROUND

Nuclear magnetic resonance is a physical phenomena which occurs when the nuclei of certain atoms are immersed in a static magnetic field and exposed to a second oscillating magnetic field. Some nuclei experience this phenomenon, and others do not, dependent upon whether they possess a property called spin. All isotopes that contain an odd number of protons and/or neutrons have a nonzero spin, making them susceptible to magnetic stimulus and therefore suitable for NMR studies. The most commonly studied nuclei are ^1H, ^{13}C and ^{19}C [1].

In nuclear magnetic resonance, nuclear spins interact with the applied external static magnetic field by aligning with it. The average alignment reflect a precession around the external magnetic field due to their nuclear magnetic moment, $\vec{\mu_i}$. This precession has a specific frequency, the so called Larmor frequency, which depends on the applied field and nuclear species:

$$\nu_L = \frac{\gamma}{2\pi} B_o \tag{1}$$

γ stands for the gyromagnetic ratio of the nucleus. The alignment of the net magnetization with the external magnetic field can be disturbed by radio frequency pulses. After a perturbation the spins realign again with

the external magnetic in a process called relaxation. An example of this realignment, after a $\pi/2$ pulse perturbation is represented in Fig. 1.

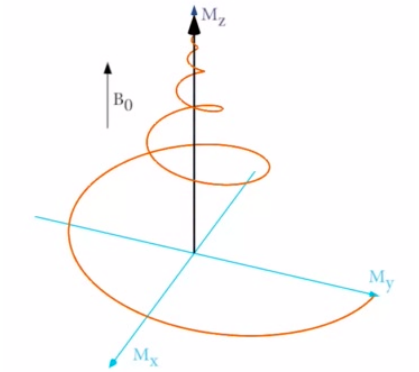

FIG. 1. Magnetization realignment with B_0, after a $\pi/2$ pulse.

The set of the Bloch equations describes this phenomenon assuming a static magnetic field $\vec{B} = B_o\vec{e_z}$ and magnetization $\vec{M} = M_o\vec{e_z}$ [2].

$$\frac{dM_x(t)}{dt} = [\vec{M} \times \gamma\vec{B}]_x - \frac{M_z(t) - M_o}{T_1} \quad (2)$$

$$\frac{dM_y(t)}{dt} = [\vec{M} \times \gamma\vec{B}]_y - \frac{M_x(t)}{T_2} \quad (3)$$

$$\frac{dM_x(t)}{dt} = [\vec{M} \times \gamma\vec{B}]_z - \frac{M_y(t)}{T_2} \quad (4)$$

The time constants T_1 and T_2 related to the realignment of nuclei magnetizations with the external field are called relaxation rates and nuclear magnetic resonance experiments are precisely used to acquire frequency dependence of relaxation rates.

The spin-lattice relaxation time, T_1 is the time constant for the physical processes responsible for the relaxation of the components of the nuclear spin magnetization vector $\vec{M}$ parallel to the external magnetic field, $\vec{B_o}$ (z component, also named longitudinal component). Values of T_1 range from milliseconds to several seconds [3].

Spin-spin relaxation time, T_2 is at its most fundamental level the evolution time towards the decoherence of the transverse nuclear spin magnetization. Fluctuations of the local magnetic field lead to random variations in the instantaneous NMR precession frequency of different spins. As a result, the initial phase coherence of the nuclear spins is lost, until eventually the phases are disordered and there is no net xy magnetization.

The equipment proposed in this document, will only measure spin-lattice relaxation time, T_1.

III. FAST-FIELD-CYCLING PRINCIPLE

In principle, a field cycling NMR relaxometer has the typical configuration illustrated schematically in the following figure :

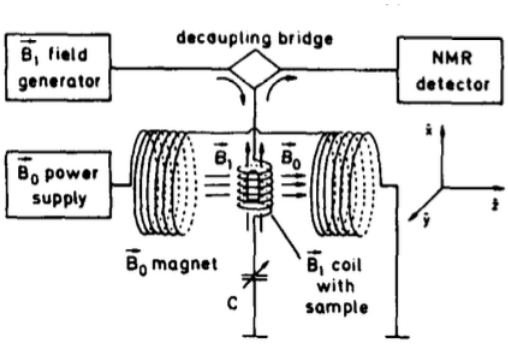

FIG. 2. Standard NMR spectrometer.

In a typical field-cycling NMR relaxometry experiment the sample is initially placed on a magnetic field, as high as possible, where it is polarized. This initial magnetic field is called polarization field, B_{oP}. Typically, it is oriented with the z axis, and forces the nuclear spin magnetization to be along , $\vec{M} = M_z\vec{e_z}$. Following this, the magnetic field is switched down to a lower value B_{oE}. In this new applied field, evolution field, the magnetization evolves to a new equilibrium, $M(B_E)$.

The final stage of the cycle, is the detection stage. The magnetic field is again increased to a high value, ,B_{oD}, with sufficient homogeneity to allow NMR signal detection, along with a $\pi/2$ RF pulse, rotating the magnetization to the xy plane. A recycle delay follows, where thermal equilibrium and polarization is reset, in order to begin the next cycle. A field cycling example can be seen in Fig [3].

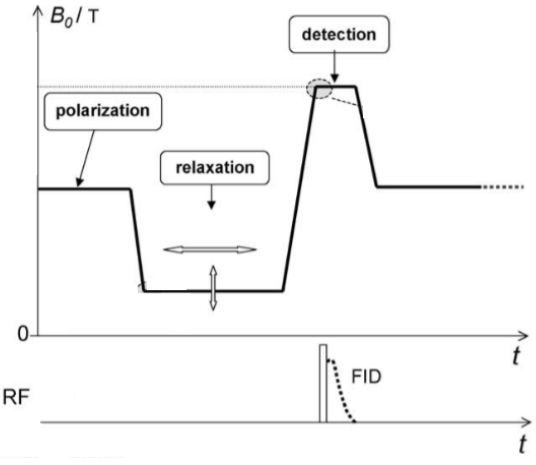

FIG. 3. Typical cycle of the main magnetic field B_o [1].

Several cycles will occur with different parameters in

order to observe the behaviour of the spin system. As the sample has to experience different intensities of B_o field, there are two methods to achieve this. Mechanically moving the sample between positions of different magnetic fields, or to change the electrical current applied to the magnet in order to vary the intensity of the field. Despite the difficulties of achieving a short steady transition ($3 - 100$ms) between fields, electronically switched field cycling is the only known alternative for measuring the shortest relaxation times.

IV. THE ELECTROMAGNET

The main component of the FFC equipment is the electromagnet. The electromagnet is the support for the main coils, provides a path for the magnetic field to flow around and also allows for the sample insertion. The electromagnet will be made of iron. Iron have a permeability in the order of 1050 compared with just 1 for air.

The electromagnet geometry will be based on the previous equipments developed in IST [4, 5]. This geometry is composed by transformer E-shaped plates. This plates are piled together in order to avoid induced currents. The electromagnet consists on two symmetrical E plates brought together with a slight cut on each of the middle feet where the sample will be accommodate. The electromagnet's height is equal to the middle feet length in order to accommodate squared coils.

In Figure 4 the electromagnet can be observed.

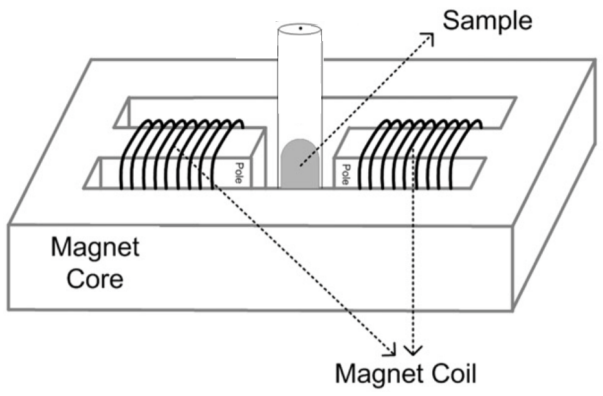

FIG. 4. Magnetic electromagnet with coils around the middle feet [5].

V. SIMULATION: COMSOL MULTIPHYSICS®

In order to define the electromagnet, a simulation using COMSOL Multiphysics® was performed.

Different physical quantities were susceptible to change influencing the characteristics of the spectrometer:

- **Ferromagnetic electromagnet size:** Different E-shaped transformer plates are available with different standard sizes, which is directly related with the electromagnet size and volume. The size of the electromagnet influence the magnetic flux density and maximum magnetic field. On one hand the smaller the electromagnet is the higher is the possible magnetic field, on the other hand the smaller is the available space for the coils limiting the number of turns and therefore the magnetic field.

- **Sample gap size:** This gap needs to the removed from the E-plates. The smaller the gap the higher will be the magnetic field magnitude at the sample site but the smaller the height of the coils will be since they are inserted through the gap. There is a minimum limit since the sample need to be heated with air and the RF coil needs to involve the sample.

- **Maximum current applied to the coils:** This is a crucial parameter since the magnetic field at sample site is directly related with the applied current. Joule heating effects must be considered as well as the fact that a higher magnetic field magnitude is created by higher currents.

- **Number of coils:** Different number of coils can be accommodated in the electromagnet depending on its size. The more coil sets the electromagnet has the higher the magnetic field is but the other limitations might arise such as cooling ability and space.

- **Number of turns in each coil:** This number should be as high as possible since it is directly related with magnetic field magnitude. It is limited by the gap size, length between E-plate feet, Joule loss effects and wire cross section.

After the evaluation of different electromagnet configurations the final decision was to built a spectrometer with the characteristics listed in Table I.

E-plate standard size	$12/13.5/15\ cm$
Number of coils	2 - 8
Number of turns per coil	$[50 - 300]$
Max. current in coils	$[0 - 5]\ A$
Minimum gap size	$15\ mm$

TABLE I. Possible range of values for the simulation.

The magnetic field in the geometry was evaluated through the simulation. The flux density and path is presented in Figure 5.

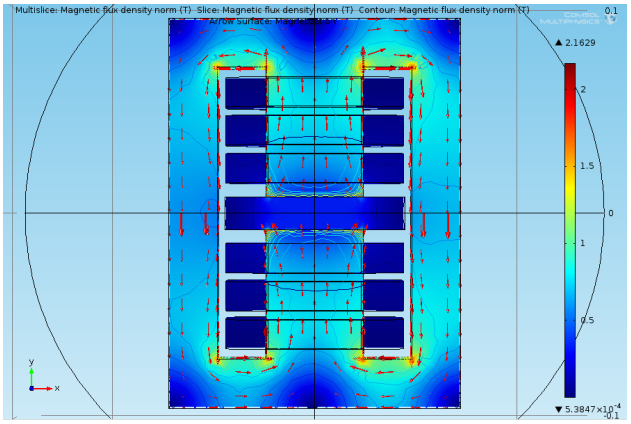

FIG. 5. Top view of magnetic field plots: Volume and Arrow line. Designed in COMSOL Multiphysics® 4.3.

VI. FIELD HOMOGENEITY

The homogeneity of the magnetic field is given by:

$$H = \Delta B / B_o \tag{5}$$

The homogeneity requirement arises from the fact that the sample needs to be polarized evenly by the same field magnitude in order for the RF pulse to match the Larmor frequency. This not only requires a uniform area in the sample site middle plane but a uniform volume. To further evaluate this volume, three planes analysed: the middle sample site plane ($y = 0$) and two additional planes in $y = \pm 0.35\ cm$

The magnetic field magnitude in the center of the planes $y = \pm 0.35\ cm$ must match the magnitude of the middle plane. Fig. 6 a) is a diagonal plot of the sample site section. Despite the divergence in magnetic field values in the limits of the section in both three planes the magnetic field magnitude converge to the 0.329 T.

In order to analyse the homogeneity, contour plots of each plane were performed in MatLab.

Two square areas were defined : the inner square (2 $cm \times 2\ cm$, A_i) and an outer square (4.5 $cm \times 4.5\ cm$, A_o) that corresponds to the sample site section. For the $y = 0$ plane (Fig. 6 b)) the magnetic field is uniform in the centered square A_i with a magnetic field of 0.3288 T in the central point. The outer square A_o presents higher non-homogeneity since it is close to the sample site section limit and the fringing effect starts to become significant.

The same method is applied to the planes $y = \pm 0.35$ cm.

In the $y = 0.35\ cm$ plane the magnetic field presented a higher uniform in the centered square A_i with a magnetic field of 0.3289 T in the central point. The outer square A_o presented high non-homogeneity. In the $y = -0.35$ cm plane the magnetic field was also uniform in the inner square A_i with a superior uniform contour line than the $y = 0$ case with a magnetic field of 0.3289 T in the central point. The outer square presents a quite different profile than the middle plane. It is concluded that in the inner square (2 $cm \times 2\ cm$) exists high homogeneity in which each layer ($y = 0$ has an homogeneity of 0.22%, $y = 0.35\ cm$ of 0.01% and $y = -0.35\ cm$ plane of 0.03%) the magnetic field magnitude is $B_{y=0} = 0.3288\ T$, $B_{y=0.35} = 0.3289\ T$ $B_{y=-0.35} = 0.3289\ T$ without existing any visible contour line in the interior. A difference in the magnetic field between the outer planes and the middle plane is observed ($\pm 0.0001\ T$). In the outer square the same can not be observed and it becomes undesirable to analyse the sample outside the inner square.

The mean values of the homogeneity are compiled next to the previous built equipment [4] in Table II. The homogeneity is proven to be acceptable with similar homogeneity results for the inner square and considerable better homogeneity in the outer square.

Plane y coordinate	Case under study	'FFC 3'
0 cm	0.22 %	0.20 %
	22.94 %	44.29 %

TABLE II. Homogeneity values compilation along the 'FFC 3' results [4]. The first line corresponds to the A_i square and the second to the A_o square.

VII. FRINGING EFFECT

The magnetic flux needs to make a transition from the iron to the air and back to the iron. This leads to a frigging effect which was observed in the simulation. The magnetic flux lines cease to be straight and parallel leading to non-uniform field.

Using the results from the simulation it was possible to plot the Fringing effect vs. gap size. This allows for an evaluation of the evolution of the fringing effect over different gap sizes. The results are plotted next to the MacLyman [6] and Roque [4] results. The expression used in this work is the same as Roque's [4], while MacLyman [6] expression is:

$$F_f = 1 + \frac{l_g}{a} ln\Big(\frac{2h}{lg}\Big) \tag{6}$$

The results are very similar in its evolution where the highest fringing factors belong to this work. The fringing factor F_f for the 1.5 cm gap case is 2.16. The fringing factor arises from an imperfectly-coupled electromagnet where leakage flux occurs. The calculated inductance is $L = 671\ mH$ with a leakage inductance of $L_L = 243\ mH$.

Such effects are not desirable at all: the leakage inductance represents a high ratio of the total inductance (36.2 %). This ratio in the previously built electromagnet corresponds to 5.5 %. The reason for such high leakage

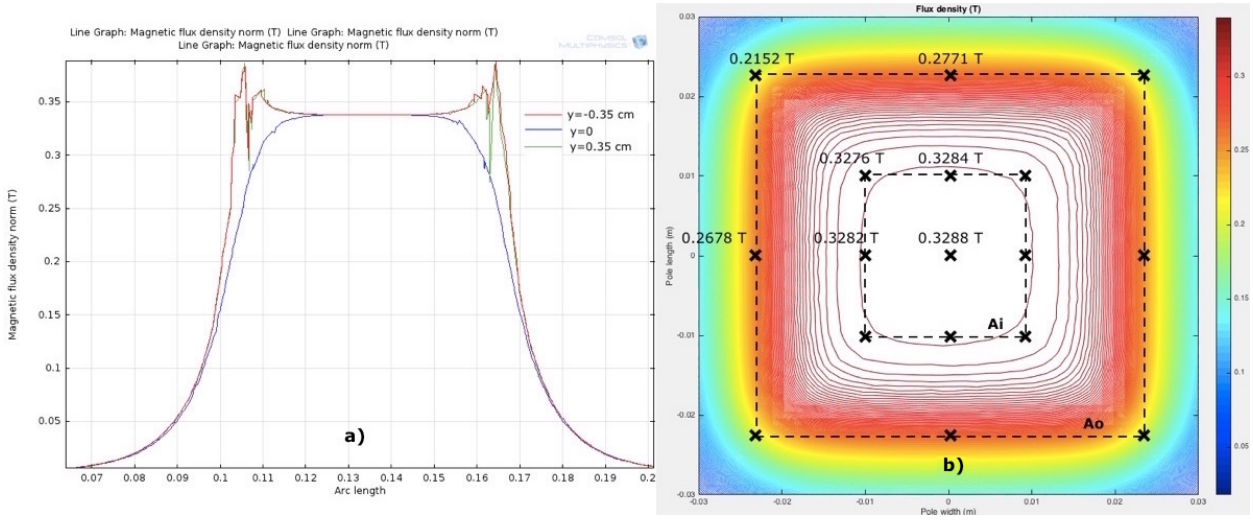

FIG. 6. a) Linear plot of the Magnetic field magnitude vs sample size diagonal for the planes $y_0 = 0$ / $y_1 = 3.5$ / $y_2 = -3.5$ mm, b) Middle plane field contour plot .

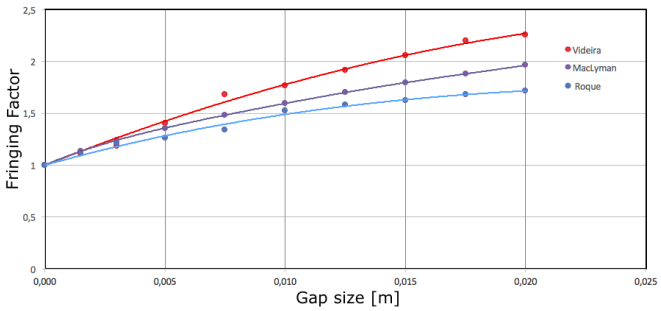

FIG. 7. Fringing factor vs. gap size for the current electromagnet, the previously built electromagnet [4] and McLyman [6].

percentage are thought to be from the smaller dimensions of the electromagnet and the proximity of the coils to the external electromagnet feet. The desire of reducing the electromagnet volume comes with the disadvantage of higher leakage flux.

The magnetic field creation leads to heating effects. This heating effects are caused by Joule losses in the coils and were evaluated in order to avoid damage or melting of the components of the system. The electrical resistance of the coils is predicted to have a total resistance of 9.3 Ω, and the total dissipated power of 84 W under a DC current of 3 A. Even though the coils will typically only be under such current in the polarization and detection phase of a fast field cycle a dissipation equivalent of constant 3 A happens when measuring the spin lattice relaxation time for a field of 0.33 T. By considering this case it is possible to overestimate the cooling requirements allowing to design a reliable cooling system. A stationary study was performed to understand the equilibrium of the system when a 3 A current is applied over large ranges of time.

Such conditions lead the electromagnet to an equilibrium temperature of 302 $°C$ without any cooling. Such temperature would irreversibly damage the coils which make it infeasible to operate the fast field cycling measurements for extended periods of time without a proper cooling system. A cooling flow was simulated, where the defined problem for the cooling effect can be summed up to: The electromagnet geometry with six coupled coils , each dissipating a total of 14 W at an initial temperature of 20 $°C$. An air laminar flow is immediately forced through the bottom of the electromagnet (in an area slightly bigger than the electromagnet's plane area) and leaves through the top (equal area of the inlet) cooling the geometry. The inlet forces air at 20 $°C$ and has a defined flow rate (m^3/s).

In order to evaluate the air flow cooling effect different flow rate were computed. The considered values of the flow rate were : 57.6 ; 80 ; 92 ; 108 ; 158 and 170 m^3/h. This was obtained after research and evaluation of different available fans in the market that could be implemented in the specific case.

The equilibrium temperatures for different flow rates are compiled in Table VII.

Flow m^3/h	Max. T. (degC)	Min. T. (degC)
57.6	64.2	49.9
80	53.4	39.4
92	49.4	35.6
108	45.9	32.4
158	38.9	26.6
170	37.9	25.9

TABLE III. Maximum and minimum equilibrium temperature in the electromagnet for a given flow rate.

VIII. EXPERIMENTAL TESTING OF THE ELECTROMAGNET

Experimental confirmation of the physical quantities provided by the simulation and analytical calculations are desired.

A. Electromagnet

The desired parameters of the electromagnet were designed and compiled. The electromagnet was built by outsourcing all the parts: from the electromagnet to the coils, and rectification of the sample site section. Two additional coils were added to serve the purpose of auxiliary coils, which compensate permanent magnetizations of the electromagnet and the earth magnetic field. This coils are composed of 430 turns each with a copper wire of 0.25 mm diameter. The built electromagnet can be seen in Figure 8.

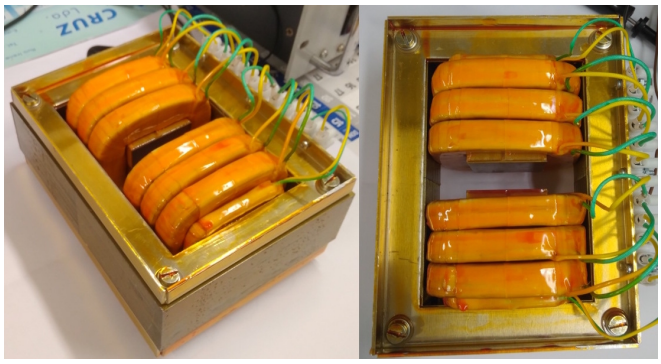

FIG. 8. Specially developed electromagnet for a NMR FFC spectrometer: 4.5 cm height built of iron standard E shaped transformer plates with 13.5 cm width, 1.5 cm gap in the middle foot, six coils with 218 turns each, maximum current of 3 A and maximum achievable magnetic field of 0.328 T.

B. Experimental measurements

1. *Coil electrical resistance*

To evaluate the total resistance of the coils a power source was used to supply the coils with an embedded multimeter in the circuit to measure the electric tension. The electrical resistance is indirectly calculated by $R = V/I$.

The experimental resistance is $9.6 \pm 0.1\ \Omega$ compared to the 9.3 Ω theoretically calculated.

2. *Coil Inductance*

The inductance of the coils come as an important parameter to measure given its relation with the current variations necessary for field cycling. A direct measurement of the inductance was performed for all the six coils with an Inductance-meter which revealed : $L = 544.5 \pm 0.1\ mH$. The auxiliary coils both measured an inductance of $L = 134.2 \pm 0.1\ mH$.

Another method was used to calculate the inductance, as well as the leakage inductance.

Two combination of coils were used: All six coils connected as usually (additive mode) and in another case half the coils fed by an opposite current in order to neutralize the field created by the other half (subtractive mode) in order to calculate the inductance L in additive mode and calculate the leakage inductance L_L with the subtractive mode.

Using the AC current method an inductance of $L = 657.7\ mH$ was obtained, and a leakage inductance of $L_L = 229.36\ mH$ which corresponds to 34.7% of the total inductance. Leakage flux is thought to arise from two factors: small electromagnet volume and proximity of the coils to the external feet. This proximity might prevent the lines to close properly and a higher distance would therefore reduce the fringing effect and leakage ratio. The first hypothesis was confirmed by the previously built electromagnet ([4]) given the lower fringing ratio (1.62 against the 2.16 of the current work) and leakage ratio (5.5% against 36.2% in the simulations) for a similar distance between feet (3 cm against the 2.25 of the current work) and a bigger electromagnet (standard plates measurement of 18 cm against 13.5 cm of the current work).

To evaluate the impact of the proximity of the coils to the external feet a new fringing factor characteristic was calculated through data obtained by COMSOL MultiPhysics®. The original distance between internal and external feet is 2.25 cm, where only a few millimetres are left between the coil and the external feet. The new characteristic was calculated for a distance between feet of 5 cm which means a distance > 2.75 cm between coils and external feet. The fringing ratio vs. gap size of the built electromagnet case (2.25 distance between feet), the 5 cm distance, and the previously built electromagnet (b=18 cm and distance between feet of 3 cm) is plotted in Figure 9.

Both the fringing ratio and leakage flux present lower values for the 5 cm case than the current case. Despite the confirmation of the contribution of the feet distance to the fringing effect and flux leakage, Roque's characteristic reveals that the main contributor for the high leakage ratio is the volume of the electromagnet.

C. Magnetic field magnitude measurement

The magnetic field magnitude over multiple planes vs. position was obtained through the simulation and evaluated (Fig. 10). An experimental evaluation of the same kind was performed. The experimental set-up consisted in the magnetic electromagnet fed by a power supply,

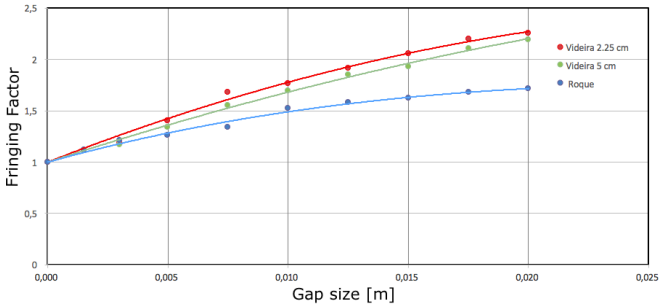

FIG. 9. Fringing ratio vs. gap size for the current case (2.25 cm distance between feet), the 5 cm feet distance, and the previously built electromagnet (b=18 cm with 3 cm distance between feet).

where both a ammeter and a voltmeter were embedded in the circuit in order to have a thoroughly evaluation of this physical quantities. A Hall Sensor (Model: GM-5180) was attached to a XY Table which controlled its position along the desired area. All the measurements were performed with the coils under a DC current of 3 A.

The magnetic field magnitude was measured in a square with total area 9×9 cm^2. This area involves the middle foot section till the beginning of the outer feet. A measurement was performed every 5 mm for a fix xx axis, followed by an increase of 5 mm in the yy axis. This resulted in a 17×17 grid and a total of 289 measured points.

Despite the efforts in making the experiment as precise as possible several factors affected its accuracy: the Hall Sensor used has temperature sensibility (the electromagnet heated considerably during the experiment) , the probe is 4 mm wide with a circular sensor of radius $1,5$ mm. This means an average calculation of the magnetic flux in such area (≈ 7 mm^2) and not in the pretended point. The XY Table distances were marked by a nail in millimetred paper which also introduces uncertainty. The alignment of the electromagnet with the probe and probe height (the electromagnet was in a standing position) was also a source of error giving the fact it was made 'by eye'. Despite of this factors the experiment allowed to confirm the range of fields around the electromagnet and the area where the fringing effect occurs confirming the predictions made by the simulation.

The Contour plot is shown next using the same method as before, but with reduced lines given the significant less number of points for this case.

The presented values of Figure 10 are an average of all the respective symmetrical points of the area of interest given their similarity in magnitude allowing for more accurate data to evaluate the homogeneity.

The same process followed for the planes : $y_1 = 3.5$ mm and $y_2 = -3.5$ mm.

The effect observed in the extremities of the sample site was already observed in the simulation (Fig. 6 a)) which corresponds to the beginning of the fringing effect. The highest magnetic field point corresponds to the middle point of the middle plane: $B_o = 0.3229$ T. The experimental data reveals similar expected homogeneity in the outer area, and relatively worst homogeneity in the inner area.

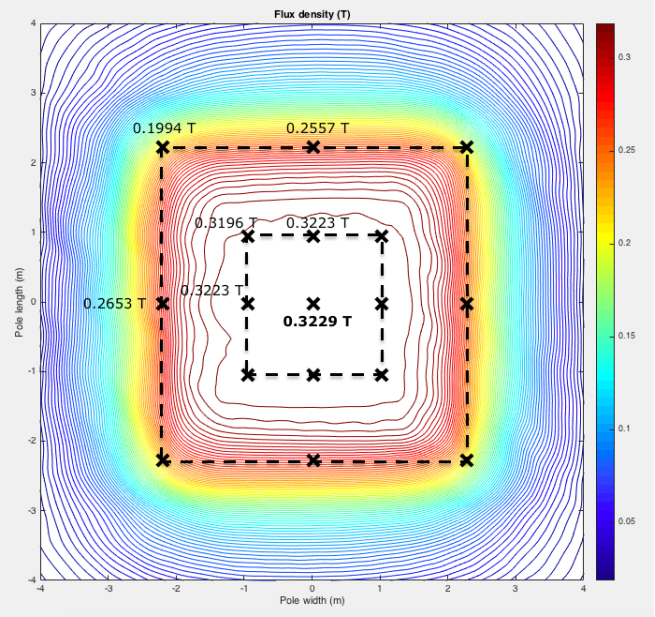

FIG. 10. Contour plot of Magnetic field magnitude vs. x&y position (z=0) using experimental data.

The volume of interested (sample placement) is the centered volume $V_1 = 2 \times 2 \times 0.7$ cm^3. The volumetric homogeneity in relation to the highest magnetic field (central point of the middle plane, $B_o = 0.3229$ T) is calculated by using the 25 point experimental points of each plane.

$$H_{V_1} = \sum_{i=1}^{75} \Delta B_i / (75 \times B_o) = 1.03\% \qquad (7)$$

IX. COUPLED SYSTEMS & SPECTROMETER ASSEMBLY

The electromagnet will operate inside a casing along with the remaining support systems which are: sample heating; cooling; RF coil.

The electromagnet was not fully built during the length of this work.

A. Sample heating

The spectrometer must be able to heat the test samples to temperatures up to 150 $^\circ C$. This is achieved by heated air and such system must be designed in order not to heat the electromagnet or other spectrometer components.

The components that constitute the heating system are: input valve, air heater, a specially designed component, glass structure, connection tubes and a thermocouple. The input valve function is to receive air at room temperature from an outer independent system and guide it to the air heater, and is yet to be defined. The air is heated by the use of a resistance in a tube. The acquired model is: Marathon-IN AH50050S. The applied power is controlled by the power supply which uses a thermocouple placed close to the sample. This allows for a precise control of the sample temperature. The specially designed component makes the hot air transition from a horizontal to a vertical flow. It also supports the next component: glass structure. This component is idealize to be similar to the one in Figure 11.

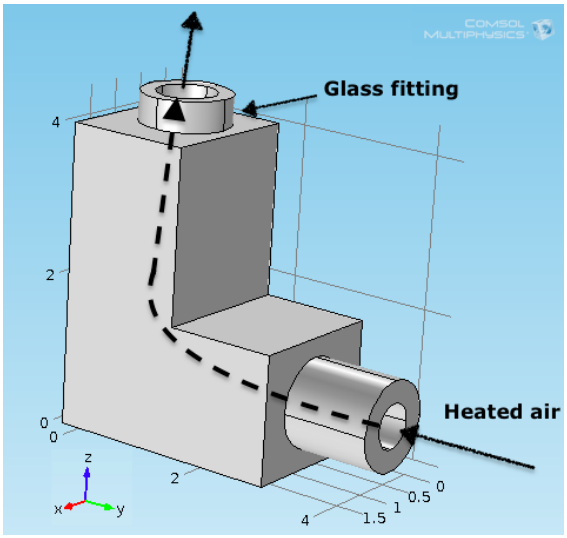

FIG. 11. Projection of the component which shifts the air flow from horizontal to vertical and is the support for the glass. Designed in COMSOL Multiphysics® 4.3 .

The glass structure is composed of two glass tubes. The inner tube has an inner and outer diameter of 8 and 9 mm, respectively. The outer tube has a 13 and 14 mm inner and outer diameter, respectively. The length of the tubes is yet to be defined. The function of the glass is to guide the air towards the sample and supporting the sample (rounded tube up to 5 mm diameter), RF coil and thermocouple. The RF coil will be place in between tubes under vacuum. The goal of creating vacuum is to prevent heat transfer between the hot air and the spectrometer, and isolate the RF coil. Connection tubes are required to connect the different components while assuring a rigid and reliable structure constituted by heat proof materials.

Pressurize air is injected into the spectrometer special valve which then leads the air to the heater, placed in the horizontal plane under the electromagnet. A connection valve - air heater is required. Another connection leads the heated air to the specially designed component forcing the flow from a horizontal to a vertical flow, into the glass structure. The glass structure where the sample is placed leads the air to exit the spectrometer through the top while heating the sample.

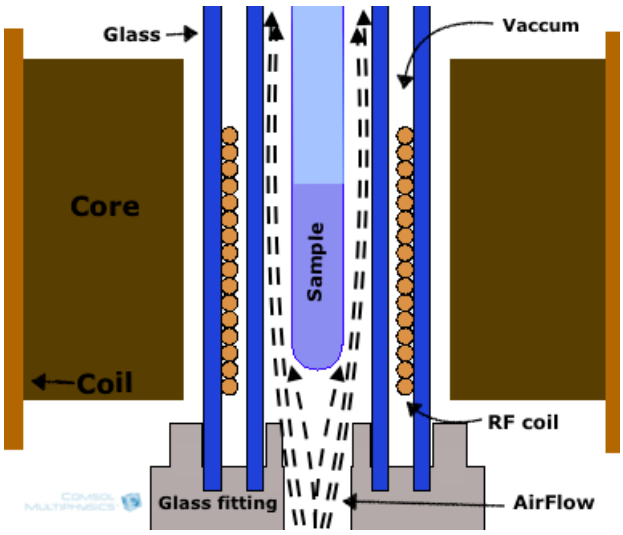

FIG. 12. Close up of the heating system. The figure is not to scale.

Different considerations are required for this system. The connection valve - air heater is to be made by a flexible tube of any material as long as the connection is reliable and well coupled in both ends but the connection between the end of the air-heater to a component yet to be designed leads air at high temperature and an according material must be used. This component is required to have a rigid structure able to provide a steady support of the glass, to handle high temperatures and to be fixed on the basis of the spectrometer. Positioning of the sample and RF coil must be within the volume centered in the electromagnet gap of dimensions: $2 \times 2 \times 0.7\ cm^3$ where the magnetic field presents its higher homogeneity. This is achieved by centering the glass structure according to Figure 13 (electromagnet top view) and making sure the middle of the RF coil is positioned in the center of the gap in the vertical plane.

B. Radio Frequency Coil

The Radio frequency coil allows for magnetization shifts and signal acquisition. The Radio frequency circuit is constituted by a coil and a capacitor which can both apply a RF pulse and receive NMR signals.

Despite the electromagnet is designed to reach a maximum magnetic field of $\approx 0.33\ T$ the current power supply is designed according to the previous versions of the FFC equipments. The Radio Frequency control system of the power supply is matched to the previous maximum magnetic field and Larmor frequency: $0.21\ T$ and 8.862 MHz. This means that given the available power supply the electromagnet is required to operate at a maximum field

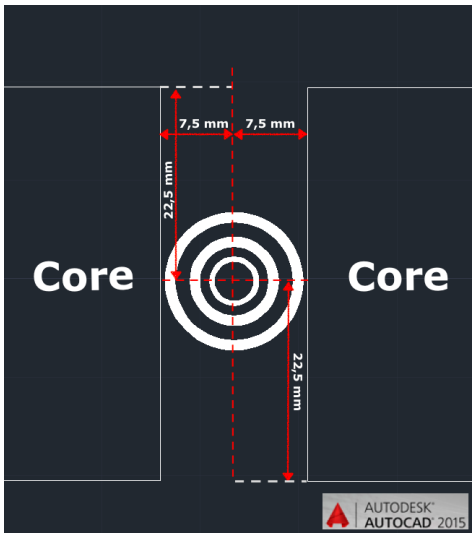

FIG. 13. Top view of the electromagnet and heating system. Centered positioning of the glass structure.

of 0.21 T and the RF generator matched to a resonance frequency of 8.862 MHz.

The coil is placed around the inner edge of the outer glass tube. It is intended to use a 0.4 mm diameter wire for the coil with 2 cm length which require 50 turns. The inductance of this coil calculated by equation 8:

$$L = \frac{N^2 \left(d/2\right)^2}{9(d/2 + 10l)} \approx 15.2\mu H \tag{8}$$

Where N is the number of turns, d the coil diameter and l the coil length. There are different possible configurations that can syncronize the RF circuit to a given frequency range being the one chosen a RLC circuit. The resonance of such circuit is given by:

$$\omega_o = \frac{1}{\sqrt{LC}} \tag{9}$$

Where C stands for the capacitance. For an inductance of 15 μH and a desired resonance frequency of8.862 MHz the capacitance is:

$$C = \frac{1}{L\omega_o^2} \approx 21.2pF \tag{10}$$

Two possible alternatives are possible to reduce the maximum magnetic field created by the electromagnet: by lowering the applied current to 2 A , or by removing two symmetrical coils (four coils should reach a magnetic field of $\approx$ 0.22 T). Reducing the current is beneficial in terms of the Joule losses (from 84 to 37 W). The removal of two symmetrical coils reduces the Joule losses (from 84 to 60 W) but also allows for bigger distance in-between coils (facilitating air cooling) and increase the distance from coils to the electromagnet gap (favoring field homogeneity).

C. Cooling System

The cooling system relies on cold air flow to assure thermal stability of the electromagnet. A vertical flow is required through the middle of the electromagnet and two openings in the casing: inlet and outlet. This openings do not require to be horizontal as long as the air flow is forced into a vertical path. The vertical flow might require to perform a downward path given the positioning of the heating system. The heating system (positioned below the electromagnet) might heat the air significantly before it reaches the electromagnet compromising the cooling effects. Further evaluation of the problem is required. The fan or fans used could be either axial or radial as long as their dimensions are small enough to fit the casing while being able to operate for long periods of time.

D. Assembly

The electromagnet and coupled systems are intended to be assembled separately from the power supply. Currently the hypothesis of using a rectangular case of similar horizontal area as the electromagnet, but with additional height is under evaluation. The electromagnet is projected to be in the middle height of the case where the cooling system is placed above the electromagnet and the heating system and remaining systems under the electromagnet.

Openings in the case are required for air inlet and outlet. The inlet has the possibility to be in the top surface of the case or in upper lateral sides. For the outlet, openings in the bottom lateral sides are feasible as long as connecting wires aren't in contact with the existing hot air. The horizontal area must be enough to correctly accommodate the heating system or extra space is necessary. An extra opening is necessary for sample insertion. The height of the case depends on the occupied volume by the heating system and cooling system. This relative positioning allows for the air to flow through the electromagnet, cooling it and the air heater ensuring thermal stability of all the components.

The power supply and pressurized air connections are to be made in the back of the spectrometer and accommodated in the bottom of the spectrometer.

X. FINAL REMARKS

The smallest FFC NMR magnet up to date was achieved, with high homogeneity in the sample site and is designed to operate within the magnetic field range of 0 and 0.33 T. Thermal effects and cooling requirements were evaluated allowing for the projection of feasible systems. The computational simulation allowed to estimate air flow rates for safe measurements over extended periods of time. The sample heating system was projected

and some components acquired and defined. The sample heating system projection allowed the definition of the RF circuit and specific coil and capacitor parameters were defined which guarantees NMR resonance conditions.

The advantages of the developed FFC magnet relatively to the generality of magnets are: reduced electromagnet's volume and weight, low power consumption, high homogeneity profile, feasible and low power cooling system.

ACKNOWLEDGMENTS

P. Videira would like to thank the supervisors of this work Pedro Sebastio, Duarte Sousa and Antnio Roque for all the good advice and knowledge. The completion of this work would have not been possible without their guidance.

[1] R. Kimmich and E. Anoardo. Field-cycling nmr relaxometry. *Progress in Nuclear Magnetic Resonance Spectroscopy*, 44(3):257 – 320, 2004. ISSN 0079-6565. doi:http://dx.doi.org/10.1016/j.pnmrs.2004.03.002. URL http://www.sciencedirect.com/science/article/pii/S0079656504000196.

[2] F. Bloch, W. W. Hansen, and M. Packard. Nuclear induction. *Phys. Rev.*, 69:127–127, Feb 1946. doi: 10.1103/PhysRev.69.127. URL https://link.aps.org/doi/10.1103/PhysRev.69.127.

[3] F. Noack. Nmr field-cycling spectroscopy: principles and aplications. *Progress in Nuclear Magnetic Resonance Spectroscopy*, 18(3):171 – 276, 1986. ISSN 0079-6565. doi: http://dx.doi.org/10.1016/0079-6565(86)80004-8. URL http://www.sciencedirect.com/science/article/pii/0079656586800048.

[4] A. Roque. *Espectrometro de RMN de CCR com utilizacao de supercondutores no magneto*. PhD thesis, Instituto Superior Tecnico, Universidade de Lisboa, 2014.

[5] Desktop fast-field cycling nuclear magnetic resonance relaxometer. *Solid State Nuclear Magnetic Resonance*, 38(1):36 – 43, 2010. ISSN 0926-2040. doi: http://dx.doi.org/10.1016/j.ssnmr.2010.07.001. URL http://www.sciencedirect.com/science/article/pii/S0926204010000457.

[6] M. C. W. T. *Transformer and Inductor Design Handbook*. Marcel Dekker, 1988.